Acoustic analysis of shock production by very high-altitude meteors—I: infrasonic observations, dynamics and luminosity

P.G. Brown[a,*], W.N. Edwards[b], D.O. ReVelle[c], P. Spurny[d]

[a]Canada Research Chair in Meteor Science, Department of Physics and Astronomy, University of Western Ontario, London, Ont., Canada N6A 3K7
[b]Department of Earth Sciences, University of Western Ontario, London, Ont., Canada N6A 5B7
[c]Los Alamos National Laboratory, Los Alamos, NM 87545, USA
[d]Academy of Sciences, Astronomical Institute, Ondřejov Observatory, 25165 Ondřejov, Czech Republic

Abstract

Four very high-velocity and high-altitude meteors (a Leonid, two Perseids and a high-speed sporadic fireball) have been unambiguously detected at the ground both optically using precision all-sky cameras and acoustically via infrasound and seismic signals. Infrasound arriving from altitudes of over 100 km is not very common, but has been previously observed for re-entering spacecraft. This, however, is the first reported detection of such high-altitude infrasound unambiguously from meteors to our knowledge. These fragile meteoroids were found to generate acoustic waves at source heights ranging from 80 to 110 km, with most acoustic energy being generated near the lowest heights. Time residuals between observed acoustic onset and model predictions based on ray-tracing points along the photographically determined trajectories indicate that the upper winds given by the UK meteorological office (UKMO) model systematically produce lower residuals for first arrivals than those from the Naval Research Laboratory Horizontal Wind Model (HWM). Average source energies for three of the four events from acoustic data alone are found to be in the range of $2 \times 10^{8-9}$ J. One event, EN010803, had unusually favorable geometry for acoustic detection at the ground and therefore has the smallest photometric source energy (10^{-5} kt; 6×10^7 J) of any meteor detected infrasonically. When compared to the total optical radiation recorded by film, the results for the three events produce equivalent integral panchromatic luminous efficiencies of 3–7%, within a factor of two of the values proposed by Ceplecha and McCrosky [1976. Fireball end heights—a diagnostic for the structure of meteoric material. Journal of Geophysical Research 81, 6257–6275] for the velocity range (55–70 km s^{-1}) appropriate to our events. Application of these findings to meteor showers in general suggest that the Geminid shower should be the most prolific producer of infrasound detectable meteors at the ground of all the major showers, with one Geminid fireball producing detectable infrasound from a given location every ∼400 h of observation.
© 2006 Elsevier Ltd. All rights reserved.

Keywords: Infrasound; Meteors; Fireballs; Meteor shower

1. Introduction and overview

Infrasonic signals generated by meteors have been detected frequently, since the first recordings were

*Corresponding author. Tel.: +1 519 661 2111;
fax: +1 519 661 4085.
  E-mail address: pbrown@uwo.ca (P.G. Brown).

made almost a century ago (cf. Whipple, 1930). Most meteor infrasound is generated by large fireballs penetrating deep into the atmosphere, with associated acoustic energy often concentrated at lower frequencies. Such low-frequency meteor infrasound may propagate and be detected for thousands of kilometers (ReVelle, 1976). Less common are acoustic detections of smaller meteors made at short (∼100 km) ranges. In the few instances where short-range meteor infrasound has been clearly detected (cf. Le Pichon et al., 2002), the meteors have been deeply penetrating and usually of modest energy. Meteor infrasound is distinct from the other type of sound occasionally associated with bright meteors, namely electrophonic or simultaneous sound (Keay, 1980). Electrophonic sound occurs simultaneously with the appearance of a meteor (unlike infrasound which propagates at acoustic velocities) and is believed to be related to emission of very low-frequency electromagnetic waves from very bright meteors (Keay and Ceplecha, 1994). Throughout our discussion when we use the term "sound" we are referring to acoustic waves, not electrophonic sound.

Generally, shower meteors associated with the Perseids of August or the Leonids of November, do not produce sounds at the ground. They are usually not energetic enough and (most importantly) ablate too high due to their fragile physical structure to easily produce the type of audible phenomena usually associated with larger meteorite-producing events. A key limitation to the detection of infrasound from such high-altitude meteors is the heavy attenuation (associated with absorptive losses from viscosity, heat conduction, turbulence and molecular relaxation) experienced by acoustic waves of high frequency (associated with smaller events) at large heights (ReVelle, 1976).

Despite this limitation, two cases of probable infrasound from shower meteors have been reported in the literature. In 1974, the infrasonic signal of a Geminid fireball observed by radar was very probably detected (McIntosh et al., 1976). In this case, an absolute correspondence between the acoustic signal and radar record was not possible due to the lack of a means of measuring the complete trajectory and position from the radar record (which provided range only). The most convincing case of a shower meteor-producing infrasound was reported by ReVelle and Whitaker (1999) associated with a Leonid fireball in 1998. In this case, a clear infrasound signal of high frequency

and short duration was detected after a bright Leonid fireball was recorded visually, with CCD cameras and probed by LIDAR (Zinn et al., 1999). While a general trajectory was determined in the atmosphere, the event did not have multi-station instrumental optical records to provide a complete path/lightcurve for reference in the infrasound analysis, limiting any numerical ray tracing. Nevertheless, it is certainly clear that the infrasound signal detected was associated with this exceptionally bright Leonid fireball, the infrasound having been generated at a height of 91 ± 7 km, and represents the first time an unambiguous acoustic signal has been detected from a shower meteor. Although this signal was brief, it demonstrated the result known from work done years ago that small sources can be detected at high altitudes if the surface winds are relatively low in speed. For example, during the NASA rocket grenade experiments in the 1960–1970s (e.g. Stroud et al., 1960), routine detection of 2–4 lb "point" source grenades at the ground became almost commonplace. These data were subsequently used to infer atmosphere temperature and horizontal wind structure in the atmosphere. This is equivalent to point source energies of 10^{-6}–10^{-5} kt, very similar to the recently quoted minimum expected to produce detectable infrasonic signals at the ground by ReVelle (2005) (1 kiloton TNT = 1 kt = 4.185×10^{12} J).

Motivated by this Leonid detection, we began to investigate the possibility of obtaining infrasonic detections of other bright high-altitude (shower) meteors. The goals of this study were to

1. Determine the expected frequency that shower (high-altitude) meteors produce infrasonic signals at the ground (for a particular station).
2. Refine from observations and theory the minimum energy needed to produce infrasonic signals at the ground from small-meteor events building on the early estimates of ReVelle (1976) and ReVelle (2005).
3. Use high-precision photographic trajectories together with ray tracing to ground-truth test several modern atmospheric models to high altitudes by comparing expected and observed acoustic arrivals from these high-altitude meteors.
4. Better understand the shock-generation mechanism producing shower infrasound signals at the ground by performing ray tracing from the high-precision trajectory measurements.

5. Make direct estimates of integral luminous efficiency for bright shower meteors by using various theoretical formulations of expected total source energy based on acoustic measurements and comparing these to the total panchromatic radiation emitted.

6. Compare theoretical models of entry to observed dynamic, photometric and acoustic measurements for large shower meteoroids to validate these models and estimate the best ablation model parameters for cm to tens of cm-sized particles.

7. Examine the seismo-acoustic coupling of airwaves from these small events.

The site chosen for the infrasonic part of the investigation was I26DE (Freyung) (48.9°N, 13.7°E) since it is an infrasonically quiet site well suited to detection of very low-amplitude infrasound signals. Additionally, it is located close to the southern edge of the European Fireball Network (EFN) (cf. Spurny, 1997), a network of cameras designed to measure the precise trajectory and brightness profile of cm-sized (and larger) meteoroids ablating in the atmosphere.

During the interval 2000–2005, we systematically searched infrasound records at I26DE for 34 European network fireballs, which had accurately measured photographic trajectories/lightcurves and occurred relatively close to I26DE (within ~300 km). Almost half of these events (16) were detected infrasonically at I26DE. In particular, 11 of these 34 events had very high ending heights (above 70 km) and of these, four were detected at I26DE. It is the infrasound from these four events (and corresponding seismic records), which constitute the material for our study.

In this first paper, we present and discuss the observational data for these four exceptionally high-altitude events based on multi-station photographic records of their flight including their trajectory solutions and photometric behavior. We also present and discuss the observed infrasound signals. Additionally, we will examine the acoustic source locations along the trajectories of the infrasound from ray tracing, make simple source energy estimates from the acoustic signals using existing relations, which have been developed and presented in other work (e.g. ReVelle and Whitaker, 1999) and establish the probable shock source mechanism (ballistic or ablational) based on ray deviations from idealized cylindrical line-source blast theory.

These acoustically derived energies are compared to the photometric lightcurves to establish among the first independent estimates for integral luminous efficiency. Finally, we conclude by examining the implications for the frequency of infrasound detection of other meteors associated with major meteor showers based on our results.

A second paper in this study will focus on an energetics analysis of these events together with numerical modeling of the blast waves, overpressure decay and meteor entry. A third and final paper will focus on the seismic recordings of the airwave from these four events and determine probable seismo-acoustic coupling efficiencies of the acoustic waves from a simple half-space model of the ground near I26DE.

2. Optical observations

A summary of the four high-altitude events that have both infrasound and ground-based photometric recordings (and in some cases spectra and seismic recordings) are shown in Table 1. Optical observations of the four high-altitude meteors were made as part of the routine operation of the EFN which employs all sky cameras equipped with fish eye lenses operating in both fixed and guided modes to record meteor activity in central Europe (cf. Spurny, 1997 for more details of network operations, goals and data reduction methods). Spectral response for the panchromatic photographic emulsion of these systems lies in the 360–675 nm wavelength band. Unless otherwise noted, all magnitude estimates refer to the panchromatic passband. Additionally, in all cases, ground-based radiometers were able to record the brightness of the meteors, within a much wider 400–1200 nm (silicon) wavelength band with a temporal sampling resolution of 1 ms. In addition to providing a precise measure of relative brightness in the silicon passband, these radiometers establish the absolute timing of each event with high precision, an essential element in linking the atmospheric trajectories to the observed airwave through ray tracings. In all four of the following cases all geodetic position, altitude, time, intensity and orbital information are derived from optical observations by the EFN.

A general property of all four events is their high velocity (greater than $60 \, \text{km s}^{-1}$), high begin and end heights (ranging from 116 to 69 km altitude) and fragile physical structure. All four move on

Table 1
Basic atmospheric trajectory data, apparent and geocentric radiants and orbital elements (J2000.0) of four bright EN meteors with high altitude infrasound registrations from all-sky photographic cameras

Meteor	EN130801	EN151101A	EN010803	EN030804
Date	13.8.2001	15.11.2001	1.8.2003	3.8.2004
Time (UT)	$23^h29^m45.0^s \pm 0.3^s$	$1^h32^m30.0^s \pm 0.3^s$	$22^h18^m54.0^s \pm 0.3^s$	$23^h10^m22.6^s \pm 0.3^s$
H_b (km)	111.43 ± 0.03	115.86 ± 0.01	109.54 ± 0.04	112.37 ± 0.02
λ_B (deg)	11.9228 ± 0.0006	13.6585 ± 0.0001	13.8620 ± 0.0003	13.27225 ± 0.00004
φ_B (deg)	49.3673 ± 0.0004	49.8103 ± 0.0001	48.8608 ± 0.0003	49.01274 ± 0.00002
H_E (km)	68.680 ± 0.010	80.86 ± 0.03	83.91 ± 0.06	75.81 ± 0.02
λ_E (deg)	11.49354 ± 0.00015	12.9998 ± 0.0004	13.0577 ± 0.0005	12.85840 ± 0.00004
φ_E (deg)	49.07426 ± 0.00010	49.8513 ± 0.0003	48.5282 ± 0.0005	48.78763 ± 0.00002
H_{max} (km)	75.5	82.2	96.1	80.9
λ_{max} (deg)	11.562	13.026	13.444	12.917
φ_{max} (deg)	49.121	49.850	48.689	48.820
L (km)	62.66	59.72	75.36	54.13
t (s)	1.06	0.84	1.09	0.90
Slope (deg)	43.03 ± 0.03	35.88 ± 0.04	19.88 ± 0.05	42.49 ± 0.02
σ_{traj} (m)	23	11	15	9
MP_{max}	-13.3	-14.9	-8.1	-12.5
Mass (g)	600	800	24	370
$\log \int I \mathrm{d}t$ (kt)	-5.25	-4.54	-6.54	-5.34
$\log E$ (kt)	-3.63	-3.31	-4.88	-3.84
PE	-5.24	-6.02	-5.27	-5.61
Type	II or IIIA	IIIB	IIIA	IIIA or IIIB
RA_{app} (deg)	51.37 ± 0.07	152.15 ± 0.03	38.88 ± 0.06	33.56 ± 0.03
DE_{app} (deg)	59.46 ± 0.03	23.47 ± 0.04	35.74 ± 0.05	54.59 ± 0.02
V_∞ (km s^{-1})	59.89 ± 0.13	71.30 ± 0.11	68.78 ± 0.10	60.8 ± 0.2
RA_g (deg)	52.08 ± 0.07	152.30 ± 0.03	39.40 ± 0.06	34.14 ± 0.03
DE_g (deg)	59.51 ± 0.03	23.30 ± 0.04	35.50 ± 0.05	54.62 ± 0.02
V_g (km s^{-1})	58.69 ± 0.13	70.18 ± 0.11	67.63 ± 0.10	59.6 ± 0.2
a (AU)	26	8.4 ± 0.7	40	24
e	0.965 ± 0.010	0.883 ± 0.010	0.976 ± 0.009	0.960 ± 0.014
q (AU)	0.9333 ± 0.0007	0.98149 ± 0.00018	0.9576 ± 0.0008	0.9668 ± 0.0005
ω (deg)	147.1 ± 0.2	169.55 ± 0.14	152.3 ± 0.2	154.7 ± 0.2
Ω (deg)	141.24775 ± 0.00001	232.73396 ± 0.00001	129.20992 ± 0.00001	131.16464 ± 0.00001
ι (deg)	111.43 ± 0.10	160.68 ± 0.07	146.74 ± 0.08	114.18 ± 0.11
Shower	Perseid	Leonid	Sporadic	Perseid

retrograde orbits of the Halley-family-type comets and are therefore unambiguously of cometary origin. Following the physical classification scheme of Ceplecha and McCrosky (1976), the mechanical properties of the fireballs can be described via the PE criterion. In the case of all four fireballs, the characteristics are those of group III (A or B); this measure establishes the meteoroids as likely having quite low bulk densities (below $1000 \, \mathrm{kg \, m^{-3}}$) and high ablation abilities (cf. Ceplecha et al., 1998 for a discussion), again consistent with a cometary origin. This fragility together with their high entry velocity is the underlying cause of their particularly high end-heights.

In what follows we provide a brief set of comments relating to each of the four meteors, beginning with the available photographic and photometric data and then presenting the associated infrasound signals for each event.

1. EN130801: *August 13, 2001 Perseid Fireball*: On August 13, 2001 a bright Perseid meteor (EN130801) was observed by the EFN at 23:29:45 UT, at its brightest the meteor reached a maximum magnitude of -13.3 (Figs. 1 and 2). Travelling initially at a velocity of $58.7 \, \mathrm{km \, s^{-1}}$, the photometric mass (using the differential panchromatic efficiency values from Ceplecha and McCrosky (1976)) was determined to be $0.60 \, \mathrm{kg}$, corresponding to an initial kinetic energy of $0.247 \, \mathrm{ton \, TNT}$. The visible trajectory of the Perseid meteor as detected by the photographic cameras had a beginning height of $111.4 \, \mathrm{km}$
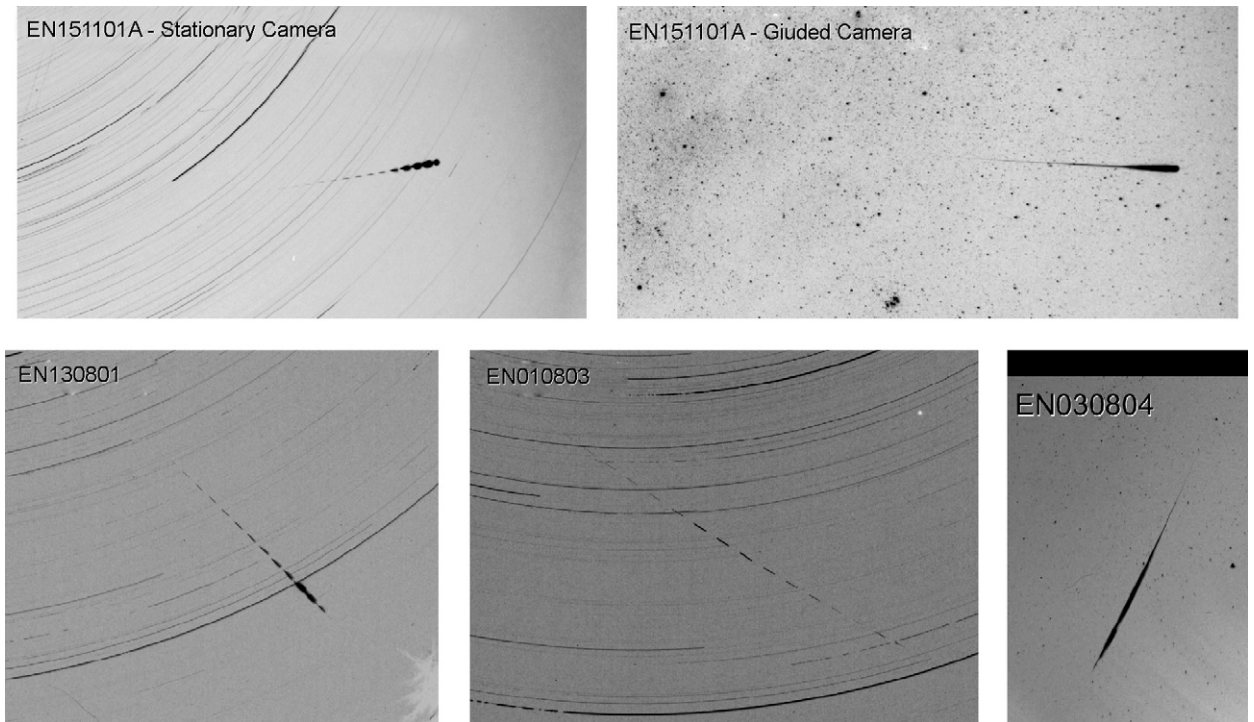
Fig. 1. European fireball network images of the four high-altitude meteors from which infrasound has also been recorded.
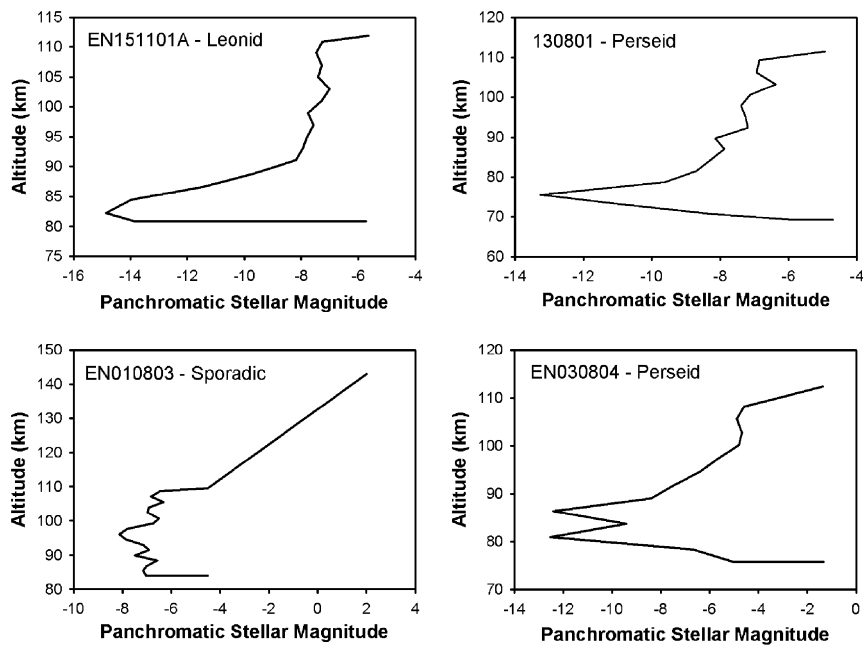

Fig. 2. Panchromatic lightcurves of all four infrasonically detected fireballs. These lightcurves were derived from densitometry measurements of the original film records following the standard technique as described in Ceplecha (1987).

and penetrated down to an end height of 69 km. In addition, records from low-light level TV (LLLTV) systems recorded the very earliest portion of the visible trajectory, beginning at 161 km altitude. The infrasound signal (described later) is clearly linked to this meteor and is the first time

infrasound from a Perseid meteor has been reported.

2. EN151101A: November 15, 2001 Leonid Fireball: At 01:32:30 UT on November 15, 2001 the EFN detected a very bright Leonid meteor traveling westwards at a heading of 275.42° and entry angle of 35.8°. Observations were made by several all-sky cameras, fixed and guided cameras (Fig. 1), a ground-based radiometer, and by spectrographic cameras at the Ondrejov observatory where a detailed meteor spectrum was obtained. The Leonid reached an absolute brightness of −14.5 (Fig. 2) during its visible descent from 120 to 81 km altitude; the event is comparable to or slightly larger in energy than the first Leonid reported infrasonically by ReVelle and Whitaker (1999). It should be noted that the extreme brightness of this event requires a large extrapolation from the brightness/density of reference stellar sources on the photograph leading to an uncertainty in the peak panchromatic magnitude of ∼1.5 magnitudes.

3. EN010803: August 1, 2003 Sporadic Meteor: This bolide event was caught on three EFN cameras on August 1, 2003 at 22:18:54 UT. With a radiant not associated with any specific major shower, it is considered a true sporadic (random) meteor. With a maximum visual magnitude of −8.1 and an initial velocity of 68.8 km s^{-1}, this sporadic meteor was found to have a photometric mass of 0.024 kg corresponding to an initial kinetic energy of 0.0136 t TNT (10^{-5} kt) and is currently the lowest mass meteoroid yet recorded with an infrasound signal at ground level. One reason for this sensitive infrasonic detection is the particular observing geometry; the visible trajectory having passed almost directly overhead of the I26DE array. In addition to these photographic data, the event was recorded by two sensitive LLLTV cameras beginning at 143 km altitude. Fig. 2 shows the panchromatic light curve.

4. EN030804: August 3, 2004 Perseid Fireball: The final high-altitude bolide event was a second Perseid meteor detected on August 3, 2004 at 23:10:23 UT and having a maximum absolute magnitude of −12.5. It had an initial photometric mass of 0.370 kg and an entry velocity of 60.8 km s^{-1}, corresponding to an initial kinetic energy of 0.163 t of TNT. Its beginning height was first observed at 114.3 km and it subsequently penetrated downward to an end height of 75.8 km. In this case, the meteor was photographed by guided and fixed all-sky cameras at EFN station 4 Churanov as close

as ∼30 km from the I26DE (Freyung) Infrasound Array.

3. Infrasound observations

The infrasound records associated with each of the four high-altitude meteor events described here are analyzed using standard techniques (cf. Evers and Haak, 2001; Edwards et al., 2006). All data were processed using the analysis package MatSeis 1.7 (Harris and Young, 1997) (available from http://www.nemre.nnsa.doe.gov/cgi-bin/prod/nemre/matseis.cgi). These measurements produce angle of arrival for the coherent infrasonic wavetrain in selected bandpasses (both backazimuth and angle of incidence or trace velocity) as well as amplitude, duration and signal cross-correlation across the array. Total signal energy is also computed, based on squaring and then summing each sample of the filtered, optimum waveform over the entire duration of the signal. More details of the methodology can be found in Edwards et al. (2006).

The I26DE infrasound array consists of five separate microbarographs (MB2000 units which measure absolute pressure changes) separated by spacings typically of order 1 km. Fig. 3 shows the layout of the I26DE array. Here, we briefly describe the salient features of each meteor-associated infrasound signal and summarize these properties in Table 2.
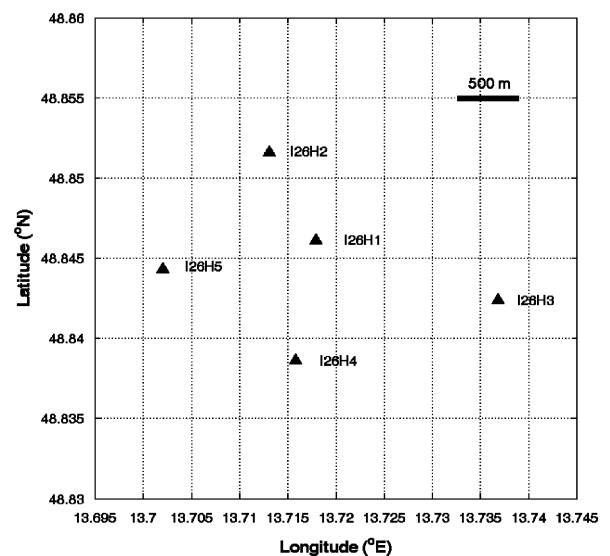

Fig. 3. The array layout for the I26DE (Freyung) infrasound station.

Table 2
Observed and computed infrasound signal properties for the four high altitude bolides as recorded at I26DE

Meteor	EN151101A	EN130801	EN010803	EN030804
Arrival time (UT)	01:40:20	23:39:32	22:24:26	23:16:03
Delay time to initial arrival (s)	470	587	332	340
Signal duration (s)	~3	~24	~28	~37
Trace velocity (km s^{-1})	0.395	0.341–0.357	0.734–1.53	0.433–0.563
Arrival azimuth (degrees)	349.5°	279°–287°	218°–242°	268°–285°
Ground range to fireball (km)	118	164	36	59
Mean signal speed (km s^{-1})	0.315	0.303	0.301	0.294
Slant range to fireball (km)	148	178	100	100
Peak to peak amplitude (Pa)	0.43±0.16	0.24±0.04	0.20±0.11	0.15±0.05
Period at maximum amplitude (s)	1.79±0.23	1.45±0.1	3.01±0.11	2.54±0.06
Integrated signal to noise ratio	36±2	64±6	32±15	45±8
Maximum cross-correlation value	0.82	0.78	0.74	0.68
Computed source height (km)	87–89	~70–95	~84–100	78–100
Blast wave radius R_0 (m)	25.0	19.6	7.7	16.8
Local air temperature (K)	272.4	303.2	303.3	302
Sound speed at ground (km s^{-1})	0.331	0.349	0.349	0.348
Observed signal incidence angle	33°	~0°	77°–39°	52°–36°

All measurements were made over the bandpass 0.3–9.5 Hz.

1. EN130801: August 13, 2001 Perseid Fireball: Infrasound from this event first arrived at the western element of I26DE starting at 23:39:32.0 UT on August 13, 2001 with a total coherent signal duration of 24 s. Observed infrasound back azimuths systematically changed from 279° to 287° during the course of the signal and are consistent with acoustic radiation emanating from the region that surrounds the flare near the end of the trail (Fig. 4). The waveform (Fig. 5) shows three distinct arrivals—an initial pressure decrease followed 5 s later by a shocky blastwave signature and then a final pressure drop another 4 s later. The individual features (labeled 1, 2 and 3 in Fig. 5) have arrival azimuths of 284.5°, 290.7° and 290.8°, respectively, indicating the endpoint detonation may be related to the initial pressure drop (which also has the smallest acoustic distance to the station). The propagation is all counter-wind based on our best model estimates (see later) and is associated with an average signal speed of 0.303 km s^{-1}. The trace speed also indicates the acoustic signal was traveling nearly parallel to the ground; presuming the signal comes largely from the detonation near the endpoint (consistent with the azimuth arrival estimates) the apparent elevation above the ground of the fireball terminal point as seen from I26DE was only 23° elevation, confirming this interpretation (see details in section on ray-trace results).
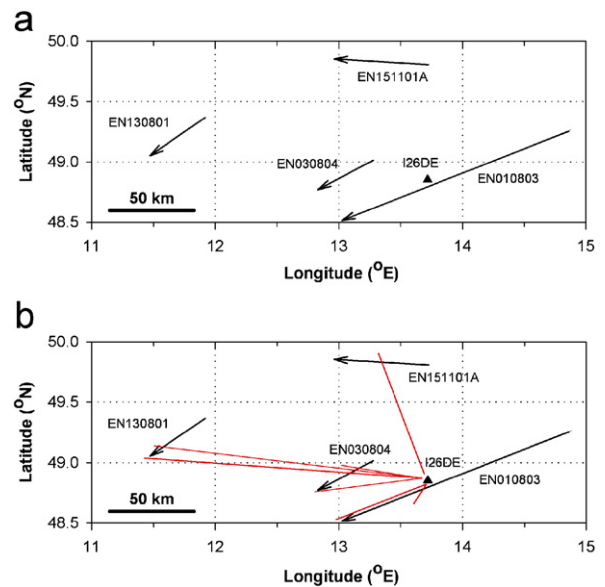

Fig. 4. Trajectories and detection geometry for the four high altitude meteors in relation to I26DE. (a) Meteors and the observing station, (b) same, with the range of observed infrasonic backazimuths for each meteor indicated. Prevailing winds for each observation were from easterly directions, except EN151101A, which were westerly.

2. EN151101A: November 15, 2001 Leonid Fireball: The acoustic signal from this energetic event begins at 01:40:20±1 UT, some ~8 min after the optical registration of the fireball. The brief blastwave infrasonic signal was recorded at I26DE and lasted only ~3 s (Fig. 5). Despite the brief duration,
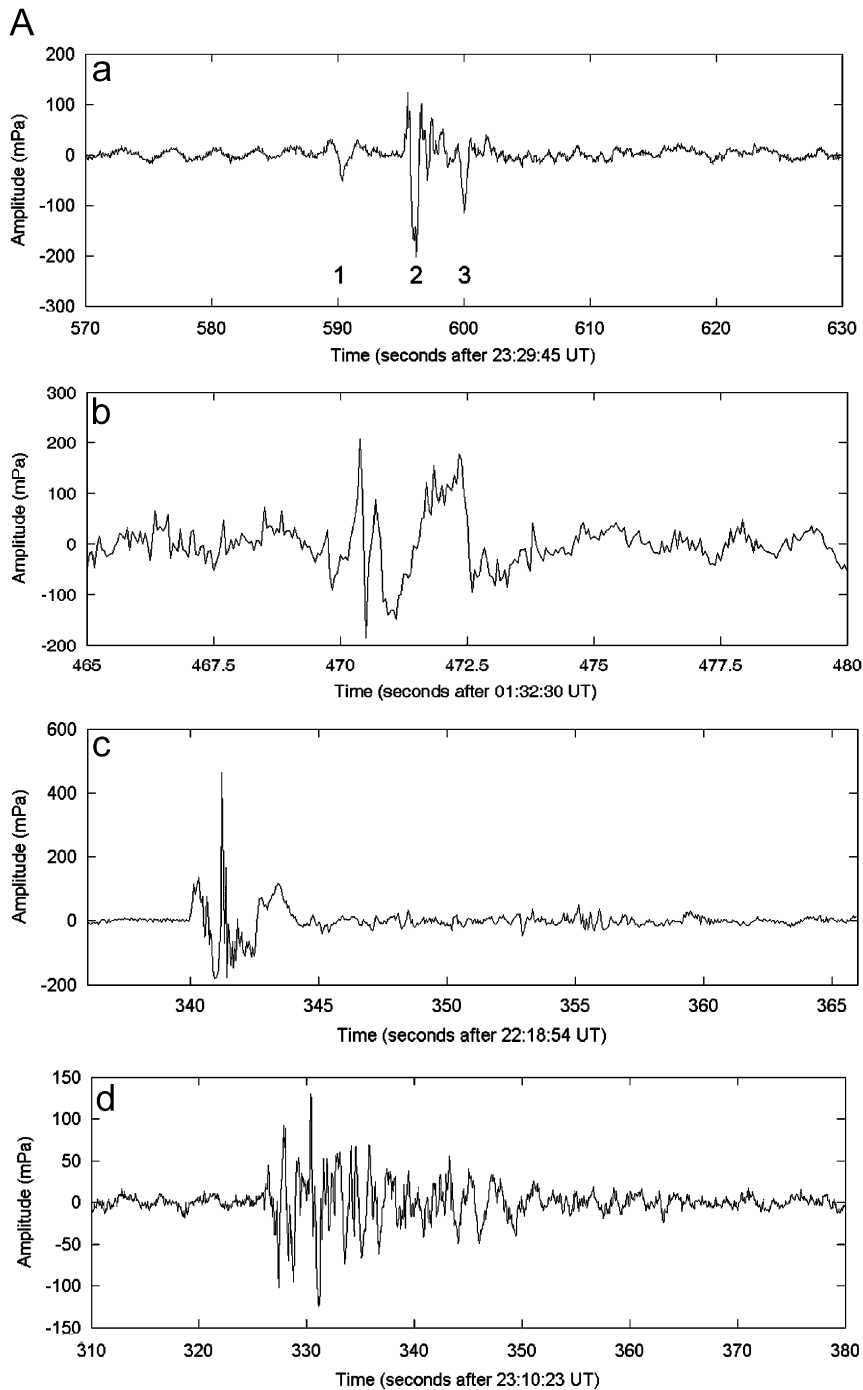
Fig. 5. (A) (TOP) Infrasonic pressure waves as recorded by the I26DE microbarometers (channel 2): (a) EN130801, (b) EN151101A, (c) EN010803 and (d) EN030804. (B) (BOTTOM) Infrasound analysis for the EN151101A meteor. Shown are (top) the unbounded F-statistic which measures coherency of the waveform across the receivers (cf. Evers and Haak, 2003), apparent trace velocity of signal across the array (middle) and the dominant arrival azimuth for signals in each of the 10 s bin windows. The solid vertical line indicates the timing of the signal arrival.
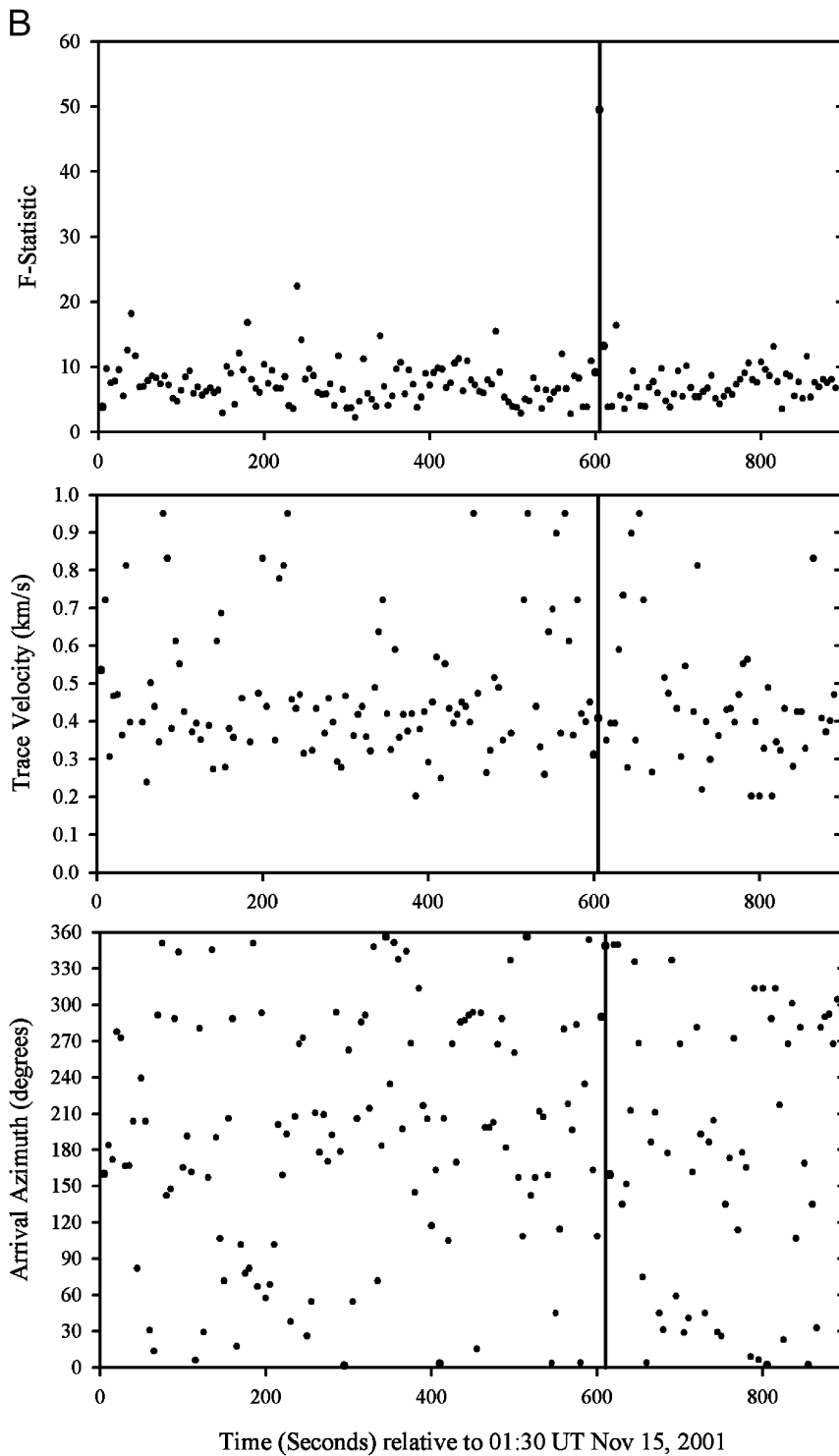
Fig. 5. (*Continued*)

the signal amplitude is the largest of the four events in this study with a backazimuth of $349 \pm 2°$ and a trace velocity of $0.395 \, \mathrm{km \, s^{-1}}$ corresponding to an arrival angle of $33°$ from the horizontal. For comparison, the apparent angular altitude of the fireball endpoint as seen from I26DE was also $33°$.

The straight-line backazimuth projection intersects the trajectory at a height of ~100 km, though this does not take into account changes due to winds (Fig. 4). The average signal speed was 0.315 km s⁻¹. The signal characteristics, including duration, frequency content and pulse shape are very similar to the infrasonic signal for the bright Leonid reported by ReVelle and Whitaker (1999) and are summarized in Table 2.

3. EN010803: August 1, 2003 Sporadic Meteor: Infrasound from this meteor first arrived at I26DE at 22:24:26 UT, some 332 s after the optical event and displayed an initial arrival back azimuths starting near 218° increasing to 230°. The arrival trace velocities ranged from 0.734 to 0.951 km s⁻¹, corresponding to very steep airwave arrivals. This is all consistent with a line source passing nearly directly over the station as indicated by the optical record, which has the meteor at an altitude near 105 km when passing closest to the station. The arrival directions further suggest I26DE detected only acoustic radiation from the last ~10 to 15 km of the path. Fig. 4 shows the arrival azimuth range and direction relative to the meteor ground path. The initial shocky *N* wave is consistent with the notion that this is the detonation point/deepest terminal point, while the signal just a few seconds after this point is very low in amplitude as might be expected for acoustic signals having been generated at >100 km altitude. Time delays of some of the weaker features after the main signal are consistent with arrival azimuths of ~230°, indicating potentially slightly higher source altitudes than the first arrivals.

4. EN030804: August 3, 2004 Perseid Fireball: This event showed a signal at I26DE beginning at 23:16:03 UT with a corresponding signal duration of 37 s. Initial arrival backazimuths start in the range 262–268° while the final values at the end of the wavetrain are close to 285°. The trace velocity systematically increases across the signal, starting near 0.433 km s⁻¹ and ending close to 0.56 km s⁻¹ corresponding to arrival angles of ~40–50° from the horizontal. The endpoint occurs near an apparent angular altitude of 45° as seen from I26DE, consistent with the acoustic arrival angles. The detection geometry, timing, trail orientation and relative wind system are almost identical to that of EN130801 (see Tables 1, 2 for comparisons of the two cases). Of particular interest to this study, the lower-frequency content of this signal (and lower amplitudes) near the end of the acoustic signal

produce back azimuths consistent with shock generation in regions on the meteor's trail where the altitudes are greater then 100 km. Fig. 4 shows the detection geometry relative to the ground projection of the trail.

The infrasonically observed characteristics of all four events are summarized in Table 2 and the filtered waveforms are shown in Fig. 5. Fig. 4 summarizes the relative geometry and detection azimuths of each meteor path relative to I26DE.

4. Ray-tracing determination of acoustic source regions

Using the infrasonic observations of arrival time and duration along with position and timing information for each meteor as summarized in Table 1 we performed ray tracings from source to receiver. As each meteor had very high-precision trajectory data (standard deviations of the trajectory solution are typically <20 m—see Table 1) the goal was to establish the portions of each trail generating acoustic signals detected at I26DE, using the photographic trajectories as the assumed starting conditions. The robustness of the source region fit was found by comparing arrival times, arrival azimuths and elevations from various heights against observed quantities at I26DE. Each of these measures is an independent check on the solution.

Once the height interval producing acoustic signals at I26DE is established for each event in this manner, it then becomes possible to find the deviation of the original acoustic radiation from pure ballistic shock (which is perpendicular to the meteor trajectory in the idealized case) and constrain whether or not the source behaves as a quasi-spherical moving point source (ablational shock). Additionally, it becomes possible to test various upper wind/atmospheric models by comparing arrival times with the predicted residuals. The raytracing was performed using both the InfraMAP software (Gibson et al, 1999) and Supracenter (Edwards and Hildebrand, 2004) software, to delimit the source regions and geometry of the observed airwaves. In general, we found almost no difference in the predicted arrival times using these two different software tools—in what follows we show only the Supracenter solution, noting that the InfraMAP solutions are virtually identical.

Using the measured position at each shutter break along each meteor's trajectory, rays were launched towards I26DE; those rays passing within

~2 km of the station were accepted as detectable and their traveltimes and launch conditions recorded. Initially, model atmospheres were constructed using nearby radiosonde releases near the time of each event (providing temperature and wind data to ~30 km altitude), supplemented with NASA and Naval Research Labs MSIS-E00 and Horizontal Wind Models (HWM) (Hedin, 1991; Hedin et al., 1996). Using these models, however, it was found that for nearly all events (except EN151101A) it was impossible to match the arrival timing of the I26DE observations. After removing all wind information, rays were again launched; however, poor timing agreement remained for three of the four events. This problem coupled with the poor agreement when winds were added, suggested potentially poor modeling of upper atmospheric winds by HWM. Indeed HWM modelled stratospheric winds in each case exceeded $80 \, \text{m s}^{-1}$ at ~65 km altitude. As these winds are easterly during the summer, the effect was to shift all predicted arrivals to later times, effectively over-correcting arrivals for the presence of winds as compared to the observed travel times exactly as observed.

In an attempt to obtain a better estimate for the stratospheric winds present during these events, we examined the UK meteorological office (UKMO) stratospheric assimilated data set which provided measurements (as taken by the UARS satellite) to an altitude of ~60 km of the temperature and wind conditions for the days in question (Swinbank and O'Neill, 1994). Satellite profiles were compared to radiosonde measurements and were found to be in excellent agreement, providing confidence for measurements at higher altitudes. Interestingly, UKMO measured wind values were approximately half of those provided by HWM at stratospheric altitudes. Thus UKMO satellite measurements were merged with MSIS-E00 and HWM model values at ~60 km and a third set of ray tracings were performed, which provided the consistently best timing fit to the observations at I26DE than either the no-wind case of the HWM modelled wind case.

Fig. 6 shows the arrival time curves for each of the four events for all three-ray tracings (no wind case, HWM and UKMO (merged with HWM above 60 km)). The differences between HWM and UKMO are significant for all events but EN151101A. In particular, HWM shows first arrivals between 15 and 30 s too late in all three of the remaining cases (reflecting the overestimation of the stratospheric winds), while the UKMO solutions

are consistent typically to within 5 s in the start residuals for these events. Given the time delays, the 5 s differences reflect average sound speeds in the UKMO data set accurate to ~1%. In what follows all timing solutions are assumed to be those solutions found using the UKMO wind data at stratospheric altitudes.

From the infrasonic signal residual times alone, as derived from the optically observed meteor trajectories, acoustic source regions for the four meteors tended to lie at altitudes $>80 \, \text{km}$. For EN151101A (Leonid) this region was found to be at 89–93 km, for EN130801 and EN030804 the source regions are more extended between ~80 and 100 km, while due to degeneracy the EN010803 (sporadic) meteor may have had contributions from heights between its terminal points at 84 km altitude up to nearly 110 km.

To refine these solutions, the ray-trace results were further examined to estimate arrival azimuths and arrival elevations as seen from I26DE. These results are shown in Fig. 7 (arrival azimuths) and Fig. 8 (arrival elevations).

The time residual solution for EN151101A, which predicts source heights of 89–93 km, is very consistent with the modelled azimuth and elevation arrivals, which supports the source height lying between 88 and 90 km, respectively. On this basis we suggest the best-fit source height for EN151101A is 89 km, with a potential range of 88–94 km (most likely near the low end of this range), lending confidence to the original source height identification from timing alone.

For EN130801, the modelled arrival elevations are near zero (horizontal) making precise determination of the best-fit height intervals problematic. Nevertheless, the modelled elevations are consistent with a first arrival from roughly near the endpoint and extending to 100 km height. The arrival azimuths are most consistent with first arrival from the endpoint near 70 km height and ending near 100 km height. Assuming the UKMO data have slightly underestimated the wind field in this counter-wind return, the timing difference of ~5 s between the modelled and observed first arrivals would suggest an overall best-fit source height from 70 to 95 km altitude.

Timing solutions for EN030804 using nominal UKMO wind parameters suggest first arrivals from near 80 km altitude. However, the presence of viable acoustic ray paths from the endpoint of this detonating fireball 2 km lower (with timing residuals
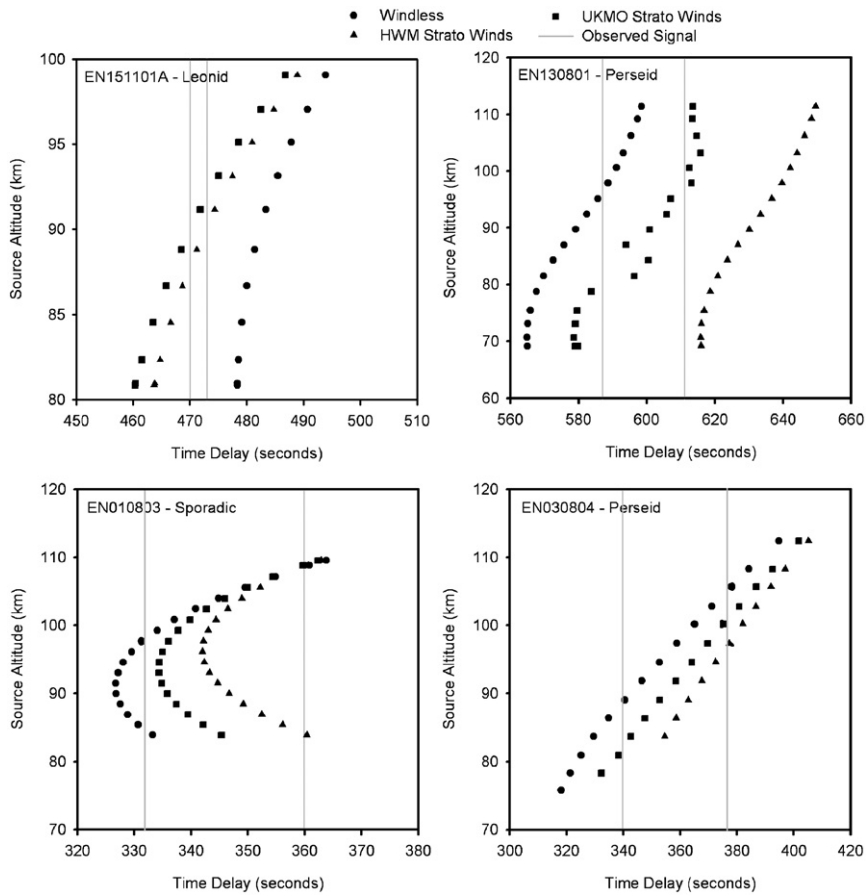
Fig. 6. Computed arrival times for acoustic rays from measured points along their respective trails for the four high altitude meteor events. Delay times bounded by gray lines indicate onset and duration of the observed infrasound at I26DE in Freyung, Germany.

of order 10 s) hints again at a possible slight underestimation of the windfield. In this case, however, the primary detonation of the fireball was observed at 81 km height, so whether the modelled winds are in error is unclear. The arrival azimuths and elevations are most consistent with first arrivals from 78 km height extending to ~100 km altitude.

Solutions for EN010803 are the most challenging due to the geometry of the trail; the meteoroid passed almost directly overhead at I26DE. The minimum in the timing model suggests first arrivals from heights near 93 km; however, the elevation arrivals are more consistent with first arrivals from near the endpoint at 84 km. Modelled azimuth arrivals show less than 1° variation from 84 to 100 km height and therefore are not diagnostic. If the elevation solutions are forced to match the observed elevation at the endpoint, all three-model signal metrics (timing, elevation and azimuth) are

consistent with the acoustic signal beginning at 105 km height.

These source height estimates/ranges are summarized in Table 2.

5. Shock mechanism identification and non-linear refraction effects

Here we present a general, approximate method to determine the refractive angle with respect to an ideal cylindrical line source (ballistic wave). This is important as it provides a semi-quantitative means of distinguishing terminal/fragmentation-type shock production (which is quasi-spherical) from cylindrical line source shock production (produced along the entire path by the body entry), which produces acoustic radiation roughly perpendicular to the meteor trajectory. Bronsthen (1983) refers to these two different shock types as ablational shocks (from fragmentation effects) and ballistic shocks. Ballistic
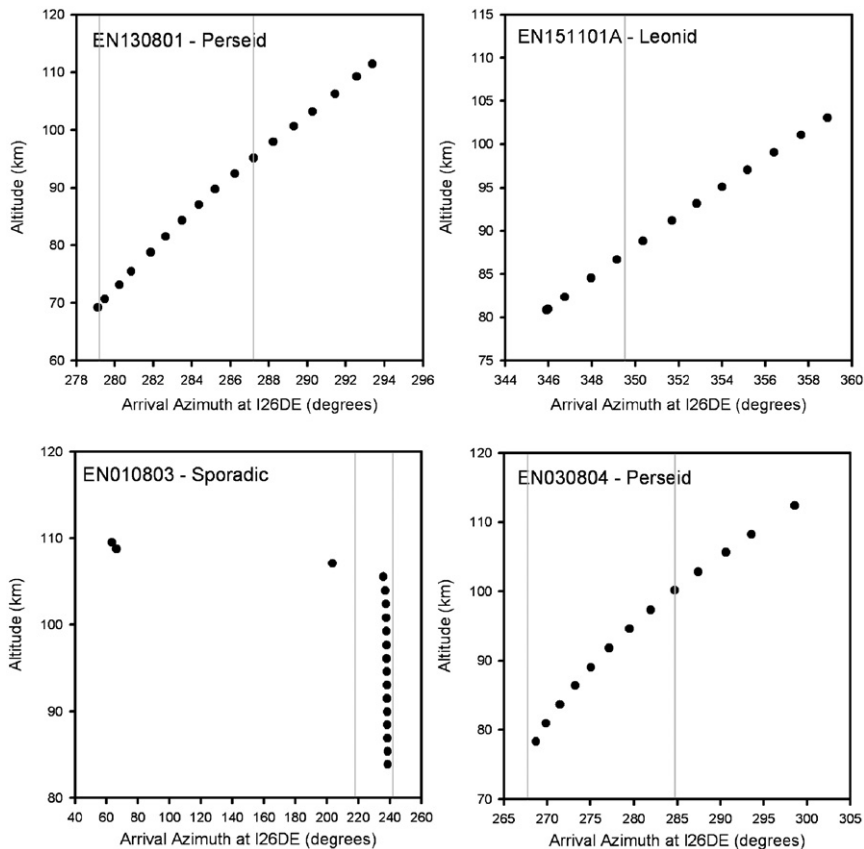
Fig. 7. Computed arrival azimuths for acoustic rays from measured points along their respective trails for the four high altitude meteor events. The range of observed arrival azimuths are shown bounded by gray lines as observed at I26DE in Freyung, Germany.

shocks produce expanding cylindrical shock fronts and therefore lead to a more confined region on the ground where acoustic radiation is detectable.

From hydrodynamic calculations with respect to the very high temperature, non-linear region (which for the line source explosion geometry lies inside one blast radius), we have extracted the computed temperatures at the radial distance where linearity approximately begins, namely at one blast radii. Interior to this distance, extreme non-linear effects dominate, though from more detailed simulations related to point source explosions, refraction is not significant in this region. We note that downward propagating rays will more quickly become linear due to the increase in air density; as these are most typically the ones observed at the ground, the analysis below should is applicable to these and not to upward propagating rays.

We make use of the numerical results of Plooster (1968) to compute the refraction at two fixed times (which can be readily converted into the adiabatic thermodynamic sound speed assuming the fluid is well mixed and behaves as an ideal gas) at one blast radii from the center of the line source.

Specific values at a fixed distance of one blast radius from Plooster's (1968) work can be summarized as follows:

$T_{peak} = 350\,K$, $T_{min} = 292\,K$ (assuming 300 K ambient background).

$C_{peak} = 375\,m\,s^{-1}$, $C_{min} = 343\,m\,s^{-1}$.

Cylindrical distance from the blast maximum to minimum (for our smallest $R_0 = 7.7\,m$) = 4.6 m.

Thus, we can obtain an estimate of $\{1/c_s\}\partial c_s/\partial z$, where z represents the vertical direction, using the absolute value of the blast radius which measured the rate at which the sound speed varies as a function of distance—if this value is close to or in excess of unity (highly non-linear), then Snell's law is not applicable.
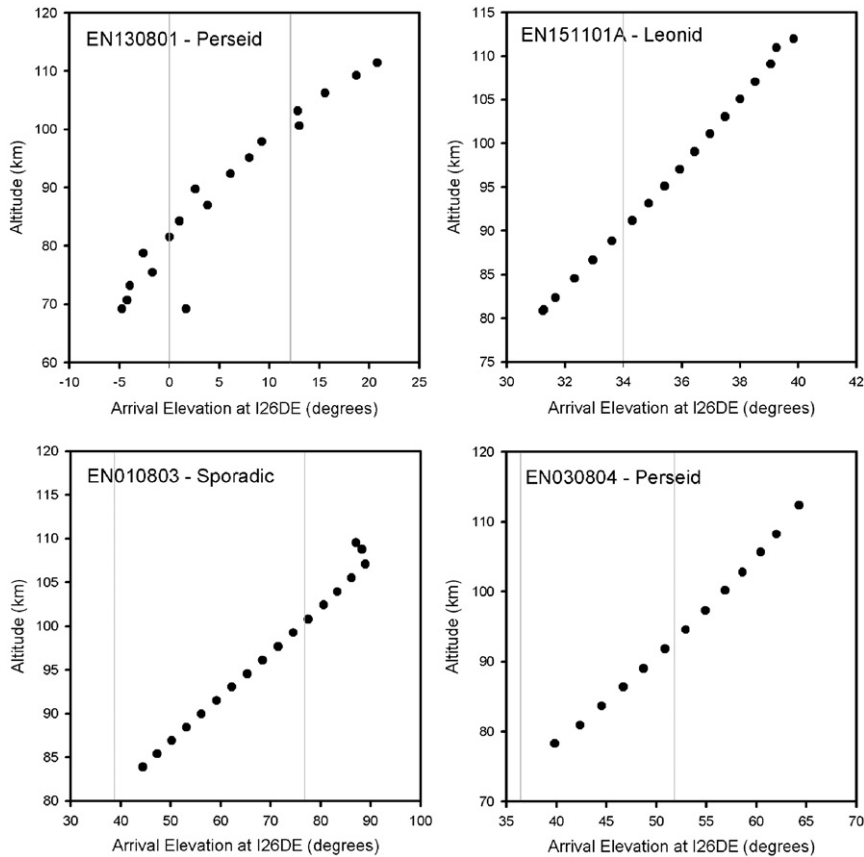
Fig. 8. Computed arrival elevations for acoustic rays from measured points along their respective trails for the four high altitude meteor events. The range of observed arrival elevations are shown bounded by gray lines as observed at I26DE in Freyung, Germany.

Moreover we may write that $c_s(z)/\cos(\theta) =$ constant. This statement assumes that a linearized Snell's law in integral form is an adequate approximation for the subsequent refraction angles. For the earliest linear part of the downward propagation using the above numerical values with $c_s(z_1) = 375\,\mathrm{m\,s^{-1}}$ and $c_s\ (z_2) = 292\,\mathrm{m\,s^{-1}}$; $z_2 - z_1 = 4.6\,\mathrm{m}$ and θ (launched from the ideal line source) $= 0°$ (i.e. perpendicular to the trail), we have that the angular deviation is $24°$ while $(1/c_s) \cdot \partial c_s/\partial z$ is $0.02\,\mathrm{m^{-1}}$. This is near the limit of the applicability of the linearity approximation which requires the gradient normalized to the sound speed to be still slowly varying and $\ll 1$. For events with larger R_0, the linearity approximation will be more valid and the angle smaller.

Thus as δc_s or $\delta T \to 0$, $\theta_{\mathrm{new}} \to \theta$ goes to $\theta = 0°$ (perpendicular to the trail), but it is not bounded as the gradients increase; we note that in reality the gradients are bounded by the possible radiation

hydrodynamics ignored in the treatment of Plooster (1968).

Applying this result to our data, the initial deviations of the modelled ray paths from each meteor trajectory were computed in order to differentiate between the two main source mechanisms of meteor infrasound; ballistic shock and fragmentation. As a result of the non-linear propagation of the initial shock rays may not be perfectly perpendicular to a meteor's trail, thus ray deviations tending to lie within ~25° of perpendicular (65–115°) were characterized as consistent with a ballistic shock source pattern from our earlier analysis.

Fig. 9 shows each individual ray-tracing point, which emanate from heights consistent with arrival times observed at I26DE. Examining the deviations for each meteor it is found that all airwave solutions are consistent with a ballistic shock radiation pattern. Only for EN030804 are the deviations
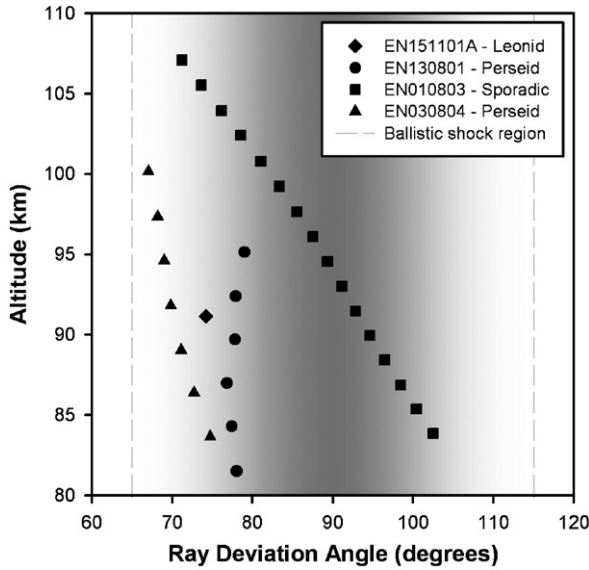
Fig. 9. Deviations of computed acoustic rays from their trajectories for those rays which arrive within the observed infrasonic signal time window. Arrival angles of 90° correspond to travel perpendicular to the meteor trajectory.

sufficiently close to the maximum expected and consistently away from the perpendicular early in the trail to suggest that a moving point source mechanism, such as fragmentation, may be a better descriptor of the airwave geometry. Even in this case, however, if the acoustic radiation is confined to the end of the trail and/or the non-linear effects slightly higher than assumed here it is entirely possible to reconcile the deviations with a ballistic solution.

6. Acoustic source energy estimation techniques: analytical/empirical approach and luminous efficiencies

The approaches which have been previously used in estimation of meteor source energies from acoustic measurements alone are summarized in ReVelle (1976), Ceplecha et al. (1998) and most recently Edwards et al. (2006). Using these previously employed analytical expressions estimates of source energy from acoustic signals alone are possible. By comparing these total acoustic energies with optical radiation emission, an independent estimate of the luminous panchromatic efficiency for each event becomes possible. As will be shown in the second paper in this series, the acoustic waves at the receiver are propagating as linear waves (having just transitioned from weak-shocks). As a result,

while the weak-shock source energy formulations derived in ReVelle (1976) are not strictly applicable to the events discussed here, the resulting energy estimates are still expected to be very close to the actual values as most of the propagation in each case occurs with the wave as a weak shock.

Valid in the weak shock regime, using observed acoustic wave period and amplitude for line sources (Ceplecha et al., 1998) leads to

$$E_s = 11.5\pi\rho_m R'^3 \left(\frac{\Delta p}{\sqrt{p_s p_g}}\right)^4 \frac{c_s^3}{V}, \qquad (1)$$

where the variables are defined below. Equivalently, the wave period method for line sources, where linear propagation is assumed after an initial weak shock phase (Ceplecha et al., 1998) produces:

$$E_s = \frac{\pi}{12}\rho_m \left(\frac{\tau}{1.579}\right)^4 \frac{c_s^7}{V} R'^{-1}, \qquad (2)$$

where E_s bolide source energy (J); ρ_m, density of the meteor (kg m^{-3}), here taken to be 1000 kg m^{-3} as appropriate to group III fireballs; Δp, observed signal overpressure (zero to peak) (Pa); p_g, ambient pressure at the ground (Pa); p_s, ambient pressure at the source altitude (Pa); c_s, average acoustic sound speed (m s^{-1}); V, meteor velocity (m s^{-1}); τ, observed period of signal at maximum amplitude (s); R', total slant range from receiver to source (m).

In addition to these purely theoretical source energy estimators, we make use of two different empirical energy estimates.

Using a data set containing a wide variety of high explosive yields (in the hundreds of tons TNT and smaller) as observed by the Los Alamos National Labs' infrasound network, Whitaker (1995) found that more generally:

$$\log E_s = 1.47 \log P_c + 2 \log R - 4.96, \qquad (3)$$

where P_c is wind corrected amplitude (Davidson and Whitaker, 1992), R is the ground range (in km) and the source energy, E_s, is in kilotons of TNT equivalent explosive energy. As with our events, this relation was constructed from experiments where infrasound readings were performed at relatively small range (few hundred km range) and with energies only one to two orders of magnitude larger than our bolide events. The primary difference between this empirical yield formulation and our data set is the point-source nature of the HE explosion data and the fact that the detonations occurred at ground level rather than at high altitude

(cf. ReVelle, 1976 for more discussion on the different acoustic signals expected between point-source and cylindrical line explosions).

Finally, we also make use of empirical relations derived from actual bolide acoustic signals as described in Edwards et al. (2006). These relations have the advantage of being most applicable to bolides (albeit generally of much larger energy than is the case for our study) and hence height of burst corrections should be smaller than is the case for Eq. (2). The primary disadvantage is that all events in the Edwards et al. (2006) study were selected based on minimum range from source to receiver of >250 km, which is comparable to or larger than most of our total slant ranges in this study. Hence, application of these relations to our events does require extrapolation and likely source energy estimation uncertainties of factors of several.

These yield equations have the form:

$$E_s = 10^{-(5.50+0.01v_h)}R^3\Delta P^{1.71}, \tag{4}$$

$$E_s = 10^{-(8.58+0.02v_h)}R^3\mathrm{SNR}^{2.08}, \tag{5}$$

where E_s is the bolide's yield (initial kinetic energy) expressed in tons (2000 lb) of equivalent TNT, R is the total slant range to the bolide in kilometers, ΔP is the maximum signal envelope amplitude (Pa), v_h is the horizontal wind between source and receiver and SNR is the integrated signal to noise ratio of the entire bolide airwave signal. More details can be found in Edwards et al. (2006).

Application of Eqs. (1)–(5) depends on measured properties of the infrasound signal, most notably signal amplitude (overpressure), the period at maximum amplitude and the integrated signal to noise ratio of the entire airwave. In general, these values will depend on the bandpass chosen for measurement and may show variation across the array due to local deviations in noise or micro-barometer differences. Note that the observed waveforms are transformed according to the provided microbarometer transfer function (one transfer function assumed to apply to all five microbarometers at I26DE). There will also be quantitative differences in a particular bandpass depending on the mode of analysis chosen; if all five signals are combined in a best-beam waveform and measurements then made, these will differ modestly from values obtained by measuring all five waveforms separately and then combining the result in an arithmetic average together with a standard deviation.

Fig. 10 shows an example of the effects of changing the lower-frequency cutoff in the filtering. As the lower frequency is moved higher, the contamination from microbaroms lessens, but some signal energy is removed and as the cutoff moves upward eventually a large portion of the signal itself is removed. The inflection in the period measurement in Fig. 10 near 0.3 Hz is due in this case to a combination of both of these effects. In this case a true period of 1.45 ± 0.05 s is adopted as this is most consistent with measurements across the lower bandpasses, before the linear decrease in period is seen above 0.35 Hz cutoff due to increasing removal of the actual signal energy. While the formal error is only 0.05 Hz, we adopt 0.1 Hz as the true physical error reflecting the uncertainty in the change in period as a function of bandpass. In practice, this level of error in period is physically insignificant in
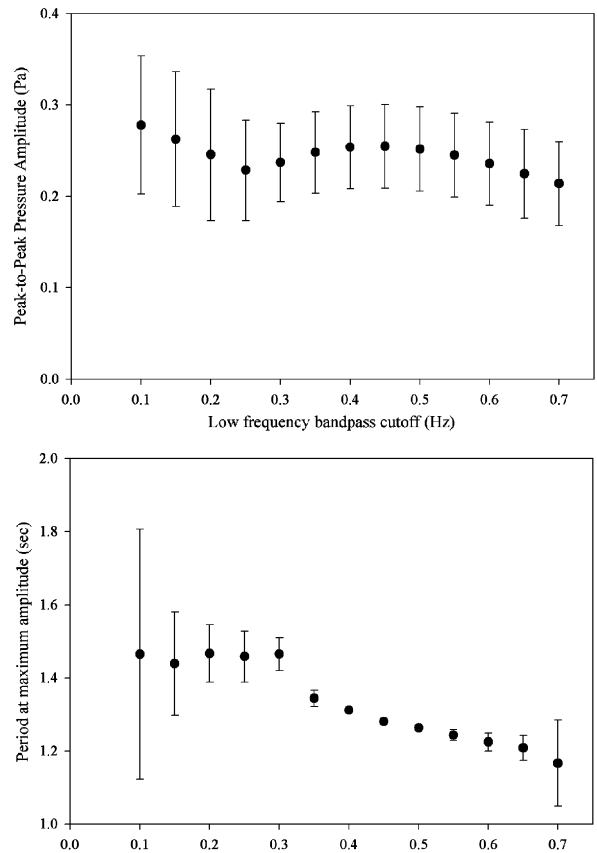

Fig. 10. The measured peak-to-peak amplitude (top) and period at maximum amplitude (bottom) as a function of lower cut-off frequency for the infrasound signal from EN130801. In each case measurements are made on the best-beam waveform, which is created by phase aligning all five microbarometer signals (see Edwards et al., 2006 for more details of the procedure).

terms of final energy estimations relative to our other uncertainties.

A similar, though less dramatic change, is seen in the peak-to-peak amplitude. With an adopted bandpass near 0.3 Hz, the amplitude is measured to be 0.24 ± 0.04 Pa. This generally reflects well the range of amplitudes over most of the chosen bandpasses. For comparison, the average amplitude of the five individual channels was found to be 0.29 ± 0.04 Pa. For all four-meteor events it was found that the variation in amplitude with band-pass, while noticeable, was not large enough to generally be outside the range of the variation between microbarometer elements using the best-beam waveform.

The final adopted values for amplitude and period (and their respective errors) are shown in Table 2. Note that the final analysis for all acoustic measurements was performed over the bandpass 0.3–9.5 Hz.

Table 3 summarizes the resulting equivalent source energies found from application of Eqs. (1)–(5) with the values from Table 2. There is a substantial range (often two orders of magnitude or more) separating these various energy estimates per event. This reflects the extrapolation of all relations used here outside their normal ranges as well as simplifications in the models which do not account for dispersion, caustics, and turbulence (cf. ReVelle, 1974 for a detailed discussion of these effects). Similar large variability has been found for source energy estimates based on direct meteor acoustic arrivals in the past (cf. ReVelle and Whitaker (1999)). In the second paper in this series we attempt to address this shortcoming of previous treatments by performing direct numerical compu-

tation of source energies from acoustic signal parameters via application of a full ablation model with more complete incorporation of real-world effects such as signal attenuation due to non-linear effects. Note that for the cases of EN130801 and EN030804 the initial acoustic arrivals associated with period at maximum amplitude and the amplitude are from near the endpoint; as a result the energy estimates using Eqs. (1) and (2) are lower limits, these energies referring to the energy deposited per unit length at the point in the trail where the acoustic emission occurs.

As a final comparison, we use the total optical radiation for each event (given by log integral $I\,\mathrm{d}t$ in Table 1) and compare to our average acoustical source energy (using all five approaches) per event. The resulting average values (with ranges in brackets) are:

τL (integral) EN151101A = 4.3% (0.7–19%),
τL (integral) EN010803 = 0.01% (0.001–0.02%),
τL (integral) EN130801 = 2.6% (0.003–12%),
τL (integral) EN030804 = 7.1% (0.01–35%).

For comparison, the often used panchromatic efficiency introduced in Ceplecha and McCrosky (1976) predicts efficiencies between 1.75% and 2.2% over the velocity range (57–71 km s^{-1}) covered by our study. From a similar detailed analysis of a bright Leonid detected infrasonically during the 1998 shower, ReVelle and Whitaker (1999) estimated an integral luminous efficiency between 0.47% and 5.3% while Borovicka and Betlem (1997) based on spectral observations estimate a luminous efficiency value near 2% for two bright Perseid meteors of similar velocity/mass to our fireballs. These are all in remarkably good agreement with the average of three of the four events;

Table 3

Summary of infrasonic energy evaluations for four high altitude meteors: all values are in units of tons of TNT equivalent energy $(4.185 \times 10^9$ J)

Type of approach	EN130801	EN151101A	EN010803	EN030804
Photographic energy (panchromatic emission ONLY)	0.0056	0.0257	0.00029	0.0046
Davidson and Whitaker (1992)—ANFO tests—Amplitude and winds (Eq. (3))	43 ± 1	4.7 ± 2.6	1.9 ± 1.5	6.4 ± 0.3
Line source (wave period): E_s (∗) (Eq. (2))	1.1 ± 0.3	3.0 ± 1.5	27 ± 4	14 ± 1
Line source (wave amplitude): E_s (∗) (Eq. (1))	0.045 ± 0.025	$3.9^{+8.4}_{-3.2}$	$4.1^{+6.0}_{-3.0}$	0.013 ± 0.010
Line source (wave period and amplitude): source height Empirical relation (Edwards et al., 2006)—Peak-to-peak amplitude (Eq. (4))	2.8 ± 0.6	0.14 ± 0.07	1.1 ± 0.5	0.68 ± 0.5
Empirical relation (Edwards et al., 2006)—Int SNR (Eq. (5))	2200 ± 0.5	4.0 ± 0.4	10 ± 7	35 ± 12

for EN010803 the unusual geometry of the detection and the erratic acoustic waveform may be the problem in producing such discordant results.

7. Lower-energy limit for meteor infrasonic detection: theory and observation

Starting from an expression relating the source kinetic energy (at any height from which the infrasound is arriving) to the non-linear line source blast wave relaxation radius of the entry, we can write the following explicit relationship for source energy (with no fragmentation effects explicitly included and a shape factor (Ceplecha et al., 1998) of $S_f = 1.209$):

$$E_s = (\pi/12) \times \rho_m \times R_0^3 \times \{c_s^3/V\}. \tag{6}$$

Or more generally written as (ReVelle, 2005):

$$E_s = 1/2m \times V^2 = [(\pi^{3/2}/2) \times (1/\{8k3\})$$
$$\times (1/S_f^{3/2})] \times [\rho_m \times R_0^3 \times \{c_s^3/V\}], \tag{7}$$

where S_f, Shape factor which reduces for a sphere ($S_f = 1.209$) Projected area/Volume$^{2/3}$; k, constant representing fragmentation effects (taken to be 0.29164); m, instantaneous meteor mass; V, instantaneous meteor velocity; R_0, instantaneous line source relaxation (blast) radius; C_s, instantaneous local adiabatic sound speed.

Application of these formulations assume that the propagation is still weak-shock, which may not be correct in some cases (see discussion in paper II), but serves as a useful approximation for our general discussion.

Observationally, Kraemer and Bartman (1981), have shown that they could readily detect a US Prairie Network bolide (P.N. no., 42556) infrasonically at the ground (at 130 km range) whose kinetic energy has been deduced from photographic data to be 1.55×10^{-5} kt with a corresponding blast wave relaxation radius of ~ 3.45 m. This bolide had an entry velocity = 16.5 km s^{-1} with a photometric mass of about 320 g and a maximum recorded magnitude of -5.1. The infrasonic signals had ~ 0.21 s period with an amplitude = 2.3 μbar (0.23 Pa), and ~ 5 s signal duration. Reverse ray tracing missed the photographed trajectory by < 410 m (with the location results triangulated from two ground-based cameras). The energy for this event is only slightly larger than our estimate for the EN010803 fireball, confirming that under excep-

tional conditions, bolides of this energy produce detectable infrasound at the ground.

From theoretical considerations, ReVelle (1976) found the minimum ground, detectable blast radius to be R_0 ($\cong$ Ma d) $\cong 10$ m. The lower limit here is due to atmospheric absorption losses at higher frequency, i.e. bolide sources with smaller R_o do not produce enough low-frequency waves to be detectable at ground level.

As shown in (6) and (7) above, the kinetic energy of the bolide is proportional to R_0 to the third power and inversely proportional to the velocity. For a spherical, cometary-type bolide with $V = 30$ km s^{-1}, $R_0 = 10$ m and a bulk density = 1000 kg m^{-3}, a minimum kinetic energy = 6.2×10^{-5} kt is predicted using $k = 1$ in Eq. (6). As will be shown from the entry dynamics solutions in paper II, most meteor sources with energies less than $\sim 10^{-6}$ kt cannot penetrate deeply enough to produce a line source blast wave (requiring continuum flow conditions to be met) to be detected at the ground and typical shower meteors (with visual magnitudes of $+2$) have kinetic energies more than 10^8 times smaller. Only exceptional meteor shower fireballs may be expected to exceed this minimum energy criterion.

8. Frequency of infrasound from meteor shower bolides

We have shown that it is possible under nearly ideal observing conditions to detect bright ($M_v < -6$) shower meteors infrasonically even if their source altitudes approach 100 km. Such bright shower meteors do not occur very often, but when they do, if the acoustic observing conditions are quite good, based on our study we may expect infrasonic arrivals at the ground as long as the entry angle is not too steep. More precisely, we may compute the approximate recurrence frequency for meteor shower infrasound from our results. Using our earlier result of $\sim 6 \times 10^{-5}$ kt as the approximate theoretical lower limit for meteor source energy to produce infrasound observable at the ground (noting that EN010803 was a factor of 6 smaller than this value, but exceptional in many respects) we can derive equivalent minimum masses required for various major showers to typically produce infrasound at the ground.

Table 4 summarizes the result of these calculations. In the table, the population index is a measure of the relative number of meteors of magnitude

Table 4
Frequency of shower infrasound

Shower	Date of maximum	Velocity (km s^{-1})	Population index	M_{lim} (kg)	MV_{lim}	Flux$_{6.5}$ ($\times 10^{-6}$ km^{-2} s)	Flux$_{infra}$ ($\times 10^{-6}$ km^{-2} s^{-1})	Frequency (h^{-1})	Hours per event
Quadrantid	3 January	41	2.1	0.30	−8.2	8.4	1.54E−10	5.55E−03	180
Lyrid	22 April	48	2.9	0.22	−8.6	4.6	4.79E−13	1.73E−05	57963
η-Aquarid	5 May	65	2.4	0.12	−9.2	6.4	6.87E−12	2.47E−04	4044
S δ-Aquarid	28 July	41	3.2	0.30	−8.2	6.2	2.33E−13	8.38E−06	119402
Perseid	12 August	60	2.1	0.14	−9.1	6	5.64E−11	2.03E−03	492
Orionid	21 October	66	2.4	0.12	−9.3	2.2	2.16E−12	7.79E−05	12841
S Taurid	5 November	27	2.3	0.69	−7.3	1	1.02E−11	3.67E−04	2726
N Taurid	12 November	29	2.3	0.60	−7.4	1.4	1.31E−11	4.73E−04	2116
Leonid	17 November	71	2.5	0.10	−9.4	1.9	8.94E−13	3.22E−05	31059
Geminid	14 December	35	2.3	0.41	−7.9	11	6.80E−11	2.45E−03	408

The shower values are derived from the compilation in Campbell-Brown and Brown (2005). Shown is the name of the shower, its approximate calendar date of maximum and entry velocity (km s^{-1}). More details are given in the text.

$M+1$ to those of magnitude M. Based on the assumed minimum energy of 6×10^{-5} kt required to produce a detectable infrasound signal at the ground, a minimum mass is given for each shower. Similarly, an approximate peak absolute magnitude based on the mass–magnitude–velocity relation from Jacchia et al. (1967) is shown. The shower flux at the peak of activity to a limiting magnitude of $+6.5$ is also given and assuming the population index remains fixed from $+6.5$ to the limiting infrasonic magnitude an equivalent flux for larger potentially infrasound-producing fireballs in each stream is computed in the Flux_infra column. Finally, the two last columns show the expected frequency of infrasound detections from any one location (assuming a collecting area out to 100 km range) and the number of hours between infrasound-producing fireballs from a particular shower at one location. Note that the frequency is an upper limit as it assumes the flux at the time of the peak, whereas most locations see a somewhat lower flux as a result of radiant geometry (the radiant is rarely overhead at the precise time of the shower). Additionally, this figure makes no allowance for acoustic detectability at the ground due to ray propagation. As a result, in practice the frequency is likely a factor of ~ 5 lower on the peak night of any given shower than shown in the table. The values quoted are for the time of maximum activity of each stream (which may be just a few hours as with the Quadrantids, to $\sim$day for the Perseids/Geminids).

The table suggests that of the annual showers, the Geminids and Perseids are most prolific at producing infrasonic signals detectable at the ground amongst the major meteor showers. This result is further strengthened by the fact that both of these showers have long-lived periods of strong activity (several days above 1/2 strength). The peak rate is highest for the Quadrantid shower of January, but its very short duration implies that the practical detection rate is more than one order of magnitude lower than shown integrated over the entire day of the maximum.

As a final remark, it is notable that the very brightest shower meteors on record have masses of order a few kilograms and peak magnitudes near $M_v = -15$, these belonging to the Leonids (cf. Spurny et al., 2000). However, at the high altitudes of ablation for such Leonids fireballs (extreme end heights no lower than 70 km; Spurny et al. (2000)) all high frequency (> 20 Hz-audible) acoustic signals will be removed through absorption before

reaching the ground (cf. Temkin, 1981). Thus, it is certainly not possible to detect audibly the sonic boom from even the brightest Leonid fireballs. Similar considerations apply to other fast group III meteor showers for which similar large ending heights apply (Perseids, Eta Aquarids, Orionids etc.). However, for slower showers with among the strongest (highest density) meteoroids such as the Geminids (group I; Spurny, 1993) which have been recorded with masses approaching 10 kg, there are cases of bright events penetrating as deep as 40–50 km altitude (Halliday et al., 1996). For these rare shower events, it is possible that weakly audible sonic booms might be heard at the surface of the Earth under ideal conditions.

9. Summary and conclusions

We have shown in this paper that acoustical propagation of waves emanating from bright meteors ablating at altitudes close to 100 km is possible provided the source is large enough (and thus has a sufficiently low-peak wave frequency). The minimum detected source energy of our four high-altitude bolides was $E = 10^{-5}$ kt, though this was possible probably due only to unusual observing geometry; in practice we suggest the minimum detectable meteor energy is closer to 6×10^{-5} kt. Shower meteors may produce such bright events roughly once per 400 h (such as the Geminids) referenced to their peak activity. In most cases audible sonic booms will not be heard from even the brightest shower meteors (due to their high ablation altitudes). The possible exception is the Geminids, where low-end heights and large initial masses may produce weakly audible sounds under ideal conditions.

A comparison of the arrival times for each event with ray-trace modeling consistently shows larger residuals when the HWM stratospheric atmospheric model winds are used as compared to UKMO winds. From this work, we suggest that the magnitude of the stratospheric winds, in particular, are too high in HWM (nearly double the values found in the UKMO model).

For all four high-altitude events, the character of the shock production is consistent with a ballistic (cylindrical) shock as opposed to the quasi-spherical acoustic radiation expected for fragmentation-type shock production. This is unsurprising given the relatively small mass (<1 kg) of the fireballs studied.

Integral luminous efficiencies were independently computed by comparing the total panchromatic radiation emitted by each event with the average acoustic source energies determined by several independent methods. This results in values between 2 and 7%, approximately a factor of two within the bounds adopted by Ceplecha and McCrosky (1976) who derived luminous efficiencies through comparison of dynamic and photometric masses.

A detailed application of an entry model and incorporation of non-linear propagation effects to better relate source energies to observed acoustic metrics is the subject of the second paper in this study series. A final paper will examine in detail the seismo-acoustic coupling of the airwaves from each meteor event.

References

Borovicka, J., Betlem, H., 1997. Spectral analysis of two Perseid meteors. Planetary and Space Science 45, 563–575.

Bronsthen, V.A., 1983. Physics of Meteoric Phenomena. Reidel, Dordrecht, New York.

Campbell-Brown, M., Brown, M., 2005. Meteors. In: Gupta, R., (Ed.), The observer's Handbook of the Royal Astronomical Society of Canada, University of Toronto Press, pp. 216–218.

Ceplecha, Z., 1987. Geometric, dynamic, orbital and photometric data on meteoroids from photographic fireball networks. Bulletin of the Astronomical Institutes of Czechoslovakia 38, 22–234.

Ceplecha, Z., Borovicka, J., Graham Elford, W., ReVelle, D.O., Hawkes, R.L., Porubcan, V., Simek, M., 1998. Meteor phenomena and bodies. Space Science Reviews 84, 327–471.

Ceplecha, Z., McCrosky, R.E., 1976. Fireball end heights—a diagnostic for the structure of meteoric material. Journal of Geophysical Research 81, 6257–6275.

Davidson, M., Whitaker, R.W., 1992. Miser's Gold, LA-12074-MS, Los Alamos National Laboratory Report, pp. 1–28.

Edwards, W.N., Hildebrand, A.R., 2004. SUPRACENTER: locating fireball terminal bursts in the atmosphere using seismic arrivals. Meteoritics and Planetary Science 39, 1449–1460.

Edwards, W.N., Brown, P., ReVelle, D.O., 2006. Estimates of meteoroid kinetic energies from observations of infrasonic airwaves. Journal of Atomspheric and Solar-Terrestrial Physics 68, 1136–1160.

Evers, L.G., Haak, H.W., 2003. Tracing a meteoric trajectory with infrasound. Geophysical Research Letters 30.

Gibson, R.G., Norris, D.E., Farrell, T., 1999. Development and application of an integrated infrasound propagation modeling tool kit. In: Proceedings of the 21st Annual Seismic Research Symposium, Las Vegas, NV, USA.

Harris, J.M., Young, C.J., 1997. MatSeis; a seismic graphical user interface and toolbox for MATLAB. Seismological Research Letters 68, 307–308.

Halliday, I., Griffin, A.A., Blackwell, A.T., 1996. Detailed data for 259 fireballs from the Canadian Camera Network and inferences concerning the influx of large meteoroids. Meteoritics 31, 185–217.

Hedin, A.E., 1991. Extension of the MSIS thermospheric model into the middle and lower atmosphere. Journal of Geophysical Research 96, 1159–1172.

Hedin, A.E., Fleming, E.L., Manson, A.H., Schmidlin, F.J., Avery, S.K., Clark, R.R., Franke, S.J., Fraser, G.J., Tsuda, T., Vial, F., Vincent, R.A., 1996. Empirical wind model for the upper, middle and lower atmosphere. Journal of Atmospheric and Terrestrial Physics 58, 1421–1447.

Jacchia, L., Verniani, F., Briggs, R.E., 1967. Selected results from precision-reduced Super-Schmidt meteors. Smithsonian Contributions to Astrophysics, vol. 11 p. 1.

Keay, C.S.L., 1980. Anomalous sounds from the entry of meteor fireballs. Science 210, 11–15.

Keay, C.S.L., Ceplecha, Z., 1994. Rate of observation of electrophonic meteor fireballs. Journal of Geophysical Research 99 (E6), 13163–13165.

Kraemer, D.R., Bartman, F.L., 1981. Infrasound from accurately measured meteor trails. In: Mathews, T., Hicks, R.B. (Eds.), Proceedings International Symposium of Acoustic Remote Sensing of the Atmosphere and Oceans, V.31–V.49. The University of Calgary Press, Calgary, Alberta, Canada.

Le Pichon, A., Guerin, J.M., Blanc, E., Reymond, D., 2002. Trail in the atmosphere of the 29 December 2000 meteor as recorded in Tahiti: characteristics and trajectory reconstitution. Journal of Geophysical Research (Atmospheres), 107, CL17-1.

McIntosh, B.A., Watson, M.D., ReVelle, D.O., 1976. Infrasound from a radar-observed meteor. Canadian Journal of Physics 54, 655–662.

Plooster, M.N., 1968. National Center for Atmospheric Research Technical Note TN-37.

ReVelle, D.O., 1974. Acoustics of meteors—effects of the atmospheric temperature and wind structure on the sounds produced by meteors. Ph.D. Dissertation, University of Michigan, Ann Arbor, Michigan.

ReVelle, D.O., 1976. On meteor-generated infrasound. Journal of Geophysical Research 81, 1217–1230.

ReVelle, D.O., 2005. Recent advances in bolide entry modeling: a Bolide Potpourri. Earth, Moon and Planets 95, 441–476.

ReVelle, D.O., Whitaker, R.W., 1999. Infrasonic detection of a Leonid bolide: 1998 November 17. Meteoritics and Planetary Science 34, 995–1005.

Spurny, P., 1993. Geminids from photographic records. In: Stohl, J., Williams, I.P. (Eds.), Meteoroids and their Parent Bodies, pp. 193–196.

Spurny, P., 1997. Exceptional fireballs photographed in central Europe during the period 1993–1996. Planetary and Space Science 45, 541–555.

Spurny, P., Betlem, H., van't Leven, J., Jenniskens, P., 2000. Atmospheric behavior and extreme beginning heights of the 13 brightest photographic Leonids from the ground-based expedition to China. Meteoritics and Planetary Science 35, 243–249.

Stroud, W.G., Nordberg, W., Bandeen, W.R., Bartman, F.L., Titus, P., 1960. Rocket-grenade measurements of temperatures and winds in mesosphere over Churchill, Canada. Journal of Geophysical Research 65, 2307–2323.

Swinbank, R., O'Neill, A.A., 1994. Stratosphere–troposphere data assimilation system. Monthly Weather Review 122, 686–702.

Temkin, S., 1981. Elements of Acoustics. Wiley, New York, 515pp.

Whipple, F.J.W., 1930. The Great Siberian Meteor and the waves, seismic and aerial, which it produced. Quarterly Journal of the Royal Meteorological Society 56, 287–304.

Whitaker, R.W., 1995. Infrasonic Monitoring. In: Proceedings of the 17th Seismic Research Symposium on Monitoring a Comprehensive Test Ban Treaty, pp. 997–1000.

Zinn, J., et al., 1999. Coordinated observations of two large leonid meteor fireballs over northern New Mexico, and computer model comparisons. Meteoritics and Planetary Science 34, 1007–1016.